Eur. Phys. J. Plus (2020) 135:433
https://doi.org/10.1140/epjp/s13360-020-00427-3

THE EUROPEAN PHYSICAL JOURNAL PLUS

Regular Article

A Serpent/OpenFOAM coupling for 3D burnup analysis

Christian Castagna[1,3], **Eric Cervi**[1,3], **Stefano Lorenzi**[1,3], **Antonio Cammi**[1,3,a], **Davide Chiesa**[2,3], **Monica Sisti**[2,3], **Massimiliano Nastasi**[2,3], **Ezio Previtali**[3]

[1] Department of Energy, CeSNEF (Enrico Fermi Center for Nuclear Studies), Politecnico di Milano, Via La Masa 34, 20156 Milan, Italy
[2] Department of Physics "G. Occhialini", University of Milano-Bicocca, Piazza della Scienza 3, 20126 Milan, Italy
[3] INFN Section of Milano-Bicocca, Piazza della Scienza 3, 20126 Milan, Italy

Received: 10 May 2019 / Accepted: 29 April 2020 / Published online: 22 July 2020

Abstract In nuclear reactor analysis, a relevant challenge is to achieve a suitable global description of nuclear systems through the coupling between neutronics and thermal hydraulics. Indeed, a multi-physics approach improves the reactor safety analysis and the design of different types of nuclear systems; in addition, it allows the investigation of physical effects at different scales of time and space. In this context, a challenging task is the development of multi-physics tools to study the fuel cycle. This paper presents a modelling approach for 3D burnup analysis with the Serpent Monte Carlo code that implements an external interface for the coupling with OpenFOAM, importing material temperatures and density field. We adopt CFD to simulate thermal hydraulics for its high flexibility that simplifies the management of input data. In addition, the coupling with a Monte Carlo code assures a natural description of the different physics phenomena of nuclear reactors. We carry out the burnup calculations for one year of burnup of a PWR fuel cell, composed of an UO_2 pin surrounded by water. We compare the results to those obtained from simulations that adopt uniform temperature and density distributions. The results show that thermal hydraulics feedback influences the spatial distribution of the reaction rates over the time, leading to a remarkable effect on the nuclide density field along the radial and axial direction. In future works, we plan to extend the analysis for fuel assembly design.

1 Introduction

Over the years, a growing interest has focused on multi-physics modelling of nuclear reactors [1]. Indeed, a global description of nuclear systems may allow to investigate physical effects at different scales of time and space, in order to improve safety analysis and design for current and innovative nuclear systems. Moreover, for Generation IV Reactors (Gen IV), the determination of thermal hydraulics conditions inside the reactor core is fundamental for the safety assessment of these systems [2–5].

Focus Point on Advances in the physics and thermohydraulics of nuclear reactors edited by J. Ongena, P. Ravetto, M. Ripani, P. Saracco.

[a] e-mail: antonio.cammi@polimi.it (corresponding author)

In this context, the development of multi-physics coupling with neutronics transport codes provides an useful tool for burnup analysis. Indeed, neutronics modelling with thermal hydraulics feedback leads to evaluate the local effects of temperature distribution and other physical parameters on fuel consumption.

In recent years, different methodologies have been developed to couple thermal hydraulics and neutronics in Monte Carlo burnup codes such as Serpent [6], MCNP [7], BGCore [8], MC21 [9] and RMC [10]. They employ coupling both with internal modules [11–13] and with external dedicated codes [14–16]. Nevertheless, the simultaneous adoption of burnup and thermal hydraulics feedback is under development [17].

The employment of Monte Carlo codes is motivated by their high accuracy and flexible implementation, with respect to deterministic codes. On the other hand, the multi-physics coupling with Monte Carlo neutronics shows different challenges in burnup calculations:

- high computational cost.
- convergence and numerical instabilities from the coupling methodologies [17]
- local burnup instabilities, when the fuel is subdivided into axial regions [18]
- implementation and validation of 3D local burnup analysis.

The latter point needs a detailed explanation. In the past, validation with experimental data was carried out with 2D codes. They adopt many simplifications and need to know a priori the final burnup at different axial regions, obtained by experimental measurements in spent fuel [19]. In this way, 2D codes are run until the final burnup to get the nuclide inventory.

However, the increase in computational effort and development of multi-physics capabilities for Monte Carlo burnup codes allow the possibility to perform 3D calculations for local burnup, which lead to realistic and accurate description of the phenomena. In this way, burnup analysis can be carried out considering the operating conditions of the reactor along the entire fuel cycle (control rods position, fuel shuffling, shutdown and so on). So there is no need to know a priori the burnup to get the final nuclide inventory.

In previous studies of an experimental TRIGA reactor, ad hoc coupling of neutronics and thermal hydraulics simulations was implemented [20] and burnup calculations were performed by taking into account the local effects of spatially inhomogeneous neutron and temperature fields [21].

In this paper, we present a burnup analysis that exploits an automated multi-physics coupling between the Serpent [6] Monte Carlo code for neutronics and the OpenFOAM [22,23] toolkit for thermal hydraulics. We simulate the latter one with computational fluid dynamics (CFD) for its high flexibility that simplifies the management of input data for different reactor geometries. In addition, CFD is three-dimensional and its coupling with a three-dimensional Monte Carlo burnup code assures a natural description of the different physics phenomena of nuclear reactors.

In the multi-physics approach, we adopt Picard iterations between Serpent and OpenFOAM, in order to take into account the mutual feedback between neutronics and thermal hydraulics at different burnup steps. On the one hand, Serpent imports temperature and density fields from OpenFOAM, to run the neutron transport simulation. On the other hand, the power distribution obtained by Serpent is employed by OpenFOAM to calculate the temperature and density fields. Therefore, the heat transfer problem is solved between the solid fuel and the liquid coolant, characteristic of different reactor designs such as pressurized water reactor (PWR), sodium fast reactor (SFR) and lead fast reactor (LFR). In the past, we carried out preliminary tests of the coupling in [24,25], adopting a simplified PWR fuel cell and a single burnup region. Moreover, in [26], we employed the multi-physics approach to study the central fuel assembly of the advanced lead fast reactor European Demonstrator

(ALFRED) reactor [27] at fresh fuel conditions, carrying out code-to-code comparisons that verified the reactor design parameters. In this work, in order to assess the methodology, we implement the procedure to evaluate the local effects of thermal hydraulics on radial and axial burnup, choosing a PWR fuel cell model for demonstration purposes.

The paper is organized as follows. Section 2 shows the multi-physics modelling approach. Section 3 describes the case study simulated, with the study of instabilities in burnup calculations. Section 4 presents the results and can be divided into three parts. In the first part, we show the effects of the multi-physics coupling for thermal hydraulics and neutronics. In the second part, we present the results on local and global nuclide compositions. In the third part, we provide the computational cost of simulations and future research developments. Section 5 summarizes the conclusions.

2 Multi-physics coupling scheme

We develop an external coupling through a coupling code technique (CCT) [28]. This procedure consists in the exchange of the information between two dedicated codes for each physics that are run separately through an iterative process. In this work, we couple Serpent Monte Carlo code for neutronics and the OpenFOAM toolkit for thermal hydraulics.

On the one hand, we chose Serpent because it is particularly suitable to be coupled with external solvers [14], through a multi-physics interface that imports temperature and density fields. In addition, Serpent is a powerful tool to perform neutron transport [29] that provides built-in burnup calculations for different reactor geometries. On the other hand, we chose OpenFOAM that adopts the finite volume method (FVM) for the discretization of the partial differential equations. Indeed, the FVM is robust and flexible [30], preserving the conservation laws without requiring any particular framework as in the finite element (FE) method [31].

The multi-physics coupling, based on Picard iterations, is shown in Algorithm 1. It consists of the following statements:

a. Start from uniform temperature T_0, density fields ρ_0 and local power $q\ (T_0; \rho_0)$ (step 1 and 3).
b. Solve the neutron transport problem with Serpent, calculating (step 3): $q_n^*{=}q^*\ (T_{n-1}; \rho_{n-1})$
c. Perform an under relaxation step $q_n = \alpha\ q_n^* + (1 - \alpha)\ q_{n-1}$; α is an under-relaxation factor that stabilizes the convergence, with a constant value at each iteration between 0 and 1. In this loop, we adopt α=0.25 that we verified to be a good choice for the case study (step 4).
d. Solve the heat transfer problem by means of OpenFOAM: $T_n = T(q_n)$, $\rho_n = \rho(q_n)$ (step 5).
e. Check the convergence (step 6), calculating the relative variation β_n of the power distribution from the previous iteration *n-1* to the current one *n* (Eq. 1):

$$\beta_n = \frac{\int_V \mid q_n - q_{n-1} \mid \mathrm{d}V}{\int_V \mid q_{n-1} \mid \mathrm{d}V} = \frac{\sum_{n=1}^{N_{\text{cells}}} \mid q_n^i - q_{n-1}^i \mid}{\sum_{n=1}^{N_{\text{cells}}} \mid q_{n-1}^i \mid} \tag{1}$$

where q_i^n is the power of ith cell at the nth iteration. At the numerator and denominator, the sums are made over all cells of the mesh, N_{cells}.

If the convergence is not reached, the process restarts to the point (2). In this work, values of β_n under 1 % ($\beta_{\text{conv}} = 0.01$) are considered optimal to obtain good accuracy on temperature fields.

Algorithm 1 The multi-physics coupling scheme between Serpent and OpenFOAM.

1: **input:** T_0, ρ_0
2: **for** n ⟵ 1, 2, ..., **do**
3: **Serpent**:
$q_n^* \longleftarrow q^*(T_{n-1}, \rho_{n-1})$
4: $q_n = \alpha\, q_{n-1}^* + (1\text{-}\alpha)\, q_{n-1}$
5: **OpenFOAM**:
$T_n \longleftarrow T(q_n)$
$\rho_n \longleftarrow \rho(q_n)$
6: **if** $\beta_n < \beta_{conv}$ **then**
break
7: **end for**

We manage the coupling through a bash shell script in the Linux environment. The wrapper code implements functions that call Serpent and OpenFOAM, check the convergence and under-relax the power. Moreover, the script is capable of restarting the calculation from a determined iteration.

The settings of the simulation (such as iteration point, maximum number of iterations, minimum β_n for the convergence and relaxation factor) are written in a configuration file that is read at each iteration. Therefore, it is possible to change the parameters during the loop.

3 Thermal hydraulics and neutronics/burnup model of the case study

We implement the coupling scheme for the case study of a PWR fuel cell. It is composed of uranium dioxide (UO_2), surrounded by water and modelled with the typical parameters of a Westinghouse 17 × 17 PWR fuel assembly [32] reported in Table 1.

We set the boundary conditions (BC), reported in Table 2, modelling separately thermal hydraulics and neutronics:

- In OpenFOAM, we simulate the active region of the fuel pin for coolant and fuel material (Fig. 1). The pre-implemented solver chtMultiRegionFoam calculates the heat transfer between liquid and solid domains, through the conjugate heat transfer (CHT) [33]. We modify the solver to be suitable for the coupling with Serpent. In particular, we change the energy balance equation by including the term for the thermal power of the fuel, generated in output by neutronics. As stated in "Introduction", in a previous work [26], we tested the solver capabilities in a multi-physics coupling at fresh fuel for the central sub-assembly of ALFRED: we got a good agreement with temperature and density fields, giving a first verification of the solver in a LFR.
  In this paper, the density of the coolant is calculated by a linear dependency on the temperature, using information taken from IAPWS (International Association for the Properties of Water and Steam) [34].
  At the inlet, we set the temperature of the water to a value of 565.15 K and the velocity

Table 1 Parameters of the simulated case study

Parameter	Value
Fuel type	UO^2
Fuel density	10.45 g/cm^3
Enrichment in ^{235}U	3.2%
Pin pitch	1.26 cm
Active height	3.66 m
Fuel pellet diameter	8.19 mm
Cladding inner diameter	8.36 mm
Cladding outer diameter	9.5 mm
Cladding material	Zircaloy-4
Thermal power	65 kW

Table 2 Boundary conditions (BC) in the OpenFOAM (*top*) and Serpent (*bottom*) model

BC in OpenFOAM	Value
Inlet temperature (coolant)	565.15 K
Inlet velocity (coolant)	5.3 m/s
Outlet pressure (coolant)	15.5 MPa
Lateral faces	Symmetric
BC in Serpent	Value
Radial direction	Reflective
Axial direction	Vacuum

to 5.3 m/s. At the outlet, the pressure is fixed to 15.5 MPa [35]. At the lateral faces of the fuel cell, we set symmetric boundary condition for all thermal hydraulics parameters.
The thermal conductivity of the fuel is modelled with the FRAPTRAN correlation [36], depending on temperature distribution and burnup. In the interface between fuel and coolant, we insert two thermal resistances for cladding and gap, with thermal conductivity 16.23 $Wm^{-1} K^{-1}$ and 0.25 $Wm^{-1} K^{-1}$, respectively. They are obtained by correlations reported in [36] for temperature at around 600 K.
We describe the turbulence through the $k-\epsilon$ [37] model; the interface between fuel and coolant is modelled by wall functions [38] implemented in OpenFOAM. The mesh is composed of 96,990 cells for the coolant and of 41358 cells for the fuel. We have carried out a grid independence analysis, checking that the temperature distribution does not change with further refinement of the mesh.

- In Serpent, along the horizontal direction, we set reflective boundary condition that models an infinite lattice. Along the vertical direction, the upper plenum of 15.9 cm is modelled and filled by helium gas [39]. At the bottom and at the top of the pin, we insert axial reflectors composed of a mixture of stainless steel and water. At the reflector extremities, we set vacuum boundary condition, implying that all the outgoing neutrons are lost.

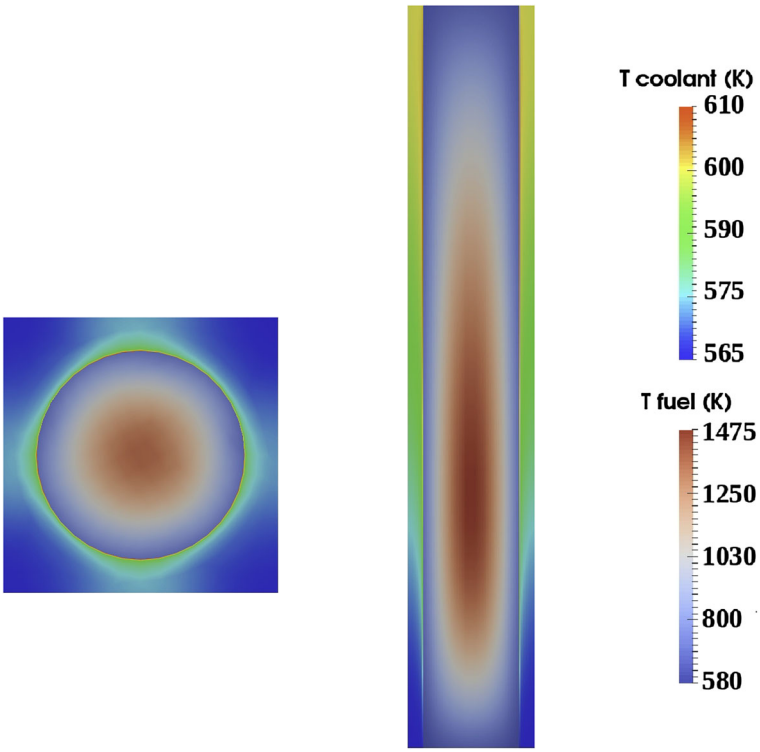

Fig. 1 Horizontal and vertical section of the fuel pin, taken by the plot of the temperature distribution during the post-processing in OpenFOAM. Red tones indicate higher temperature

3.1 Burnup analysis

At the beginning, we provide a brief description of the explicit burnup schemes implemented in Serpent, widely used by the existing Monte Carlo codes. After that, we describe the burnup analysis performed in previous studies. Then, we present the burnup analysis of this work, discussing the problem of instabilities with explicit burnup schemes and the adoption of the stochastic implicit Euler (SIE) method [18].

3.1.1 Explicit burnup schemes in Serpent

Serpent implements explicit burnup schemes to estimate nuclide densities, known as explicit Euler and predictor–corrector methods [40]. In the explicit Euler method, transport solution is obtained at the beginning of step (BOS) and reaction rates are assumed to be constant during the depleted time step. In predictor–corrector schemes, the accuracy of results is improved with respect to the previous method.

A predictor–corrector method works as follows:

a. BOS cross sections and flux are calculated by Monte Carlo neutronics.
b. BOS reaction rates are used to deplete materials, along the time step.
c. From end of step (EOS) materials composition of point b, EOS cross sections and flux are calculated by Monte Carlo neutronics.

d. BOS materials are depleted, employing the average between BOS and EOS of cross sections and flux.

The predictor step (points a and b) uses BOS cross sections and flux for the entire step, which corresponds to the constant extrapolation of the explicit Euler scheme. The corrector step (points c and d) employs a linear interpolation between BOS and predicted EOS values. Serpent also implements higher-order estimates [40] can be obtained by using the BOS values from the previous step. In this procedure, linear and quadratic fits replace the constant and linear extrapolation of the predictor and corrector steps.

3.1.2 Burnup analysis of the previous study

In preliminary studies [24,25], we carried out burnup analysis with a single depletion zone over the fuel material. We employed predictor–corrector method with LE/LI combination, based on linear extrapolated (LE) reaction rates for the predictor and linear interpolated (LI) reaction rates for the corrector calculation. We found that if we take into account the thermal hydraulics feedback on fuel consumption, the profiles of the neutron flux and reaction rate distribution are asymmetric along the axial direction, during the entire fuel cycle. Even if this study does not take into account the inhomogeneous distribution of fuel burnup, in the radial and axial direction of fuel pin, it was very useful to test the simulation and computational tools. Moreover, from the comparison with burnup simulations which adopt uniform temperature and density distributions, we found differences in the order of a few percentages for the nuclide densities of ^{235}U, ^{239}Pu and other elements, proving that thermal hydraulics feedback has nonzero effect on burnup calculations. The present paper improves the fuel cell modelling and extends the analysis to many burnup zones, to consider local effects on fuel consumption.

3.1.3 Burnup analysis of the present study

In the Serpent model of this study, we divide the pin into five radial zones of equal area and 18 axial zones of equal length, in order to perform burnup calculations for a total of 90 burnup zones.

We simulate the fuel consumption of the average pin (13.46 MWd/kgU) in a PWR with standard condition for a period of 365 days, consisted of the following steps in days: 1, 2, 7, 15, 30, 60, 90, 120, 150, 180, 210, 240, 270, 300, 330 and 365.

We carry out two burnup calculations that we call *coupled* and *uniform* case. The *coupled* case implements temperature and density fields of materials, as calculated by the Serpent–OpenFOAM coupling applied to fresh fuel and updated at 60, 120, 240 and 365 days.

The uniform case corresponds to an uniform temperature approach. In these simulations, we set the temperatures to 585 K for the coolant and 895 K for the fuel and water density to 703 kg m^{-3}. These are the mean values, calculated from the thermal and density profiles obtained by the coupling with fresh fuel. We compare the two cases to get a preliminary evaluation of thermal hydraulics feedback on fuel consumption. We use the JEFF-3.1.1 [41] library for the cross sections of the materials in transport calculations.

Numerical Instabilities of explicit burnup schemes

In [24,25], the definition of a single burnup zone allows stable calculations of fluxes and nuclide densities for predictor–corrector method. Differently, the division of the fuel in many zones could cause numerical instabilities, producing spatial oscillations of the nuclide field, as the typical xenon oscillations [42].

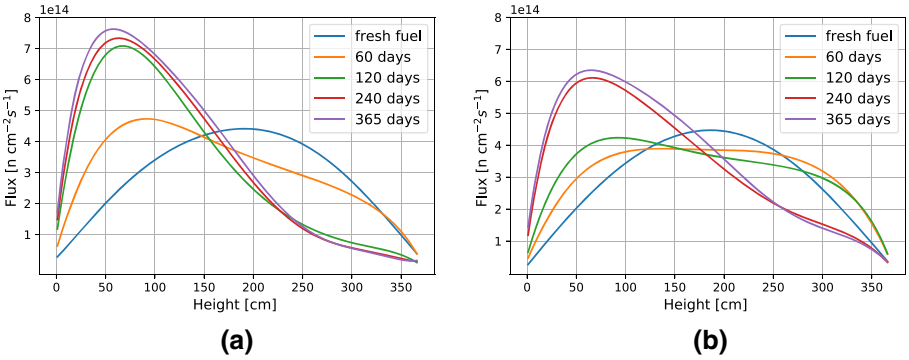

Fig. 2 Neutron fluxes at fresh fuel, 60, 120, 240 and 365 days for the *uniform* case, obtained by the explicit Euler **a** and predictor–corrector **b** methods with 2.5×10^7 neutron histories for each burnup step

We carry out preliminary simulations for uniform case to investigate this aspect. We run two burnup calculations until 365 days with the explicit Euler method and predictor–corrector method with LE/LI combination. We simulate 2.5×10^7 neutron histories at each burnup step, assuring good statistics.

In these calculations, we observe spatial instabilities of the neutron flux. Figure 2 reports the results at fresh fuel, 60, 120, 240 and 365 days. The fluxes are stable at fresh fuel. Then, they have spatial oscillations that are sharpen at 120 days for explicit Euler scheme, 240 and 365 days for both methods. The amplitude of the oscillations suggests that the errors are not statistical but due to the presence of numerical instabilities. Indeed, we also verified that the oscillations persist if we increase the number of neutron histories. As proved in paper [18], the numerical instabilities are caused mainly by different factors, such as the xenon oscillations, the number of materials and zones included in the burnup analysis, the neutron energy spectrum and the dominance ratio of the system.

The instabilities can be explained considering the mutual interaction between neutron flux ϕ and xenon distribution Π along the axial direction. For the sake of clarity, let consider Euler method, where the transport solution is obtained at the BOS and reaction rates are assumed to be constant during the time step:

- Let us suppose that Π_i is higher in the lower region at burnup step i; $\phi_i(\Pi_i)$ will be higher in the upper region owing to the absence of the neutron absorber.
- In the next step $i+1$, higher ϕ_i results in an increase of $\Pi_{i+1}(\phi_i)$ in the upper region. This leads to a higher $\phi_{i+1}(\Pi_{i+1})$ in the lower region.
- In the following steps, with the previous considerations, neutron flux and xenon distribution will oscillate until the end of burnup.

For the above explanation, we can refer to Fig. 3. It shows the oscillatory behaviour of fluxes and xenon distribution from the explicit Euler scheme, in the following steps at 270, 300, 330 and 365 days. Xenon distribution is calculated by the average over the five radial regions for each axial zone.

Through the same mechanism, instabilities of predictor–corrector methods appear in both predictor and corrector steps. The problem could be fixed by decreasing the time step, to avoid the departure of neutron flux. However, it was shown [18] that this approach is not practical because time steps of the order of few days or less are needed. If the instabilities are originated by the explicit nature of the previous burnup schemes, the solution can be reached through the adoption of implicit methods.

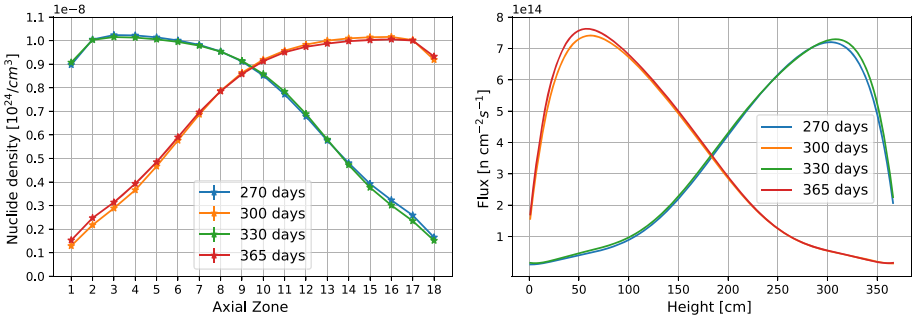

Fig. 3 Axial concentrations of ^{135}Xe **a** and neutron fluxes **b** at 270, 300, 330 and 365 days, obtained by the explicit Euler method with 2.5×10^7 neutron histories for each burnup step

The stochastic implicit Euler (SIE) method

Dufek et al. [43] have developed the stochastic implicit Euler (SIE) method that is proved to be unconditionally stable for arbitrarily large time steps, also when the thermal hydraulics conditions change during the fuel consumption [44]. The SIE method adopts a stochastic approximation with under-relaxation factor, based on the Robbins–Monro algorithm [45]. The relaxation could be applied to nuclide density or neutron flux field. The details about the mathematical derivation of the method are reported in [43].

The SIE scheme, described in [43] and implemented in Serpent, is shown in Algorithm 2 for the sake of clarity and completeness. It employs EOS values of reaction rates to calculate EOS nuclide densities. The procedure is based on the following scheme:

a. Start with nuclide density N_0 at fresh fuel and estimation of the flux ϕ_0 (steps 1 and 2).
b. Loop with several inner iterations for each ith burnup point (from steps 3 to step 12). It begins with EOS nuclide field $N_{i+1}^{(0)}$ (step 4) at the end of the time length t; M is the cross section and fission yield matrix; and D is the decay matrix. $N_{i+1}^{(0)}$ is used to calculate the neutron flux $\phi_{i+1}^{(1)}$ at the first inner iteration (step 6).
c. At each n-th inner iteration, the EOS neutron flux $\phi_{i+1}^{(n)}$ (step 6) results from the EOS density obtained by the previous iteration. The flux is relaxed calculating the mean $\overline{\phi}_{i+1}^{(n)}$ (step 7) over all fluxes ϕ_{i+1}^{j} (j=1,…,n), estimated until the current inner iteration. After that, the EOS nuclide density $N_{i+1}^{(n)}$ is continuously updated (step 8).
d. The last inner iteration calculates the final value of EOS density N_{i+1} (step 10) and flux ϕ_{i+1} (step 11) of the ith time step. The process restart to (b) for the next burnup point.

We underline that in Algorithm 2, the neutron transport solution is not obtained using the nuclide densities estimated in the last inner iteration. It follows that the final calculation of the neutron fluxes does not represent their real estimation for a specific burnup point. For this reason, the SIE method in Serpent is intended to be used to calculate only the nuclide densities. The neutron fluxes have to be simulated in separated criticality calculations that import nuclide concentration calculated at a specific burnup point.

To reach stability of burnup solution, we employ the SIE scheme for burnup analysis of this paper. We simulated 2×10^6 active neutron histories per burnup step, corresponding to 10^5 neutron histories multiplied by 20 inner iterations. Differently, when we calculated the temperature and density fields by running coupled Serpent–OpenFOAM simulations,

Algorithm 2 The stochastic implicit Euler (SIE) method in Serpent.

input: N_0
$\phi_0 \longleftarrow \phi_{B(N_0)}$
for i $\longleftarrow$ 0, 1, ..., **do**
  $N_{i+1}^{(0)} \longleftarrow N_i \exp[M(\phi_i)Dt]$
  for n $\longleftarrow$ 1, 2, ...,c **do**
    $\phi_{i+1}^{(n)} \longleftarrow \phi_{B(N_{i+1}^{(n-1)})}$
    $\overline{\phi}_{i+1}^{(n)} \longleftarrow \sum_{j=1}^{n} \phi_{i+1}^{j}/n$
    $N_{i+1}^{(n)} \longleftarrow N_i \exp[M(\overline{\phi}_{i+1}^{(n)})Dt]$
  end for
  $N_{i+1} \longleftarrow N_{i+1}^{c}$
  $\phi_{i+1} \longleftarrow \overline{\phi}_{i+1}^{(c)}$
end for

we simulate the neutron transport with 2.5×10^7 active neutron histories. We increased the neutron histories for these calculations because this statistics reaches a relative power variations under 1% after the convergence. This value assures an uncertainty less than 1° on the average fuel temperature, that is, the convergence criterion of this coupling.

4 Results

At the beginning, we present the results from the neutron transport and thermal hydraulics calculations, obtained after the convergence of the multi-physics coupling at fresh fuel, 60, 120, 240 and 365 days. Then, we show the local effects on the fuel depletion for different nuclides along the axial and radial direction. Finally, we present the results about global fuel consumption and we compare all results of the coupled case with those obtained in the uniform case.

4.1 Coupling at fresh fuel

Before running the burnup history, we apply the coupling scheme to the case study with fresh fuel. As reported in Fig. 4, a decreasing trend of the relative power variation can be seen during the first three iterations. We finally reached the convergence with a relative power variation at around 0.7%, (indicated by the dashed red line in Fig. 4) less than the tolerance of 1%. After the convergence, this value does not decrease because it depends on the statistical fluctuation of the Monte Carlo method. If we wanted to improve the accuracy, we would have to increase the number of simulated neutron histories.

After the last iteration of the coupling, OpenFOAM provides the temperature distribution of the coolant and the fuel. Figure 5a shows that the water temperature increases from the bottom (0 cm), where the injection occurs, to the top of the pin (366 cm). This effect is caused by the heating through the active zone. On the other hand, Fig. 5b shows that the thermal profile of the fuel has the maximum in the lower half, with the typical asymmetric shape of the coupling at fresh fuel [12]. Indeed, in the lower part, higher coolant density results in more effective moderation of neutrons, thus increasing the effective cross section of fission reactions. This is explicitly shown by the asymmetric axial profiles of fission rate and neutron flux, reported in Fig. 6a and b, obtained from the transport calculation in Serpent.

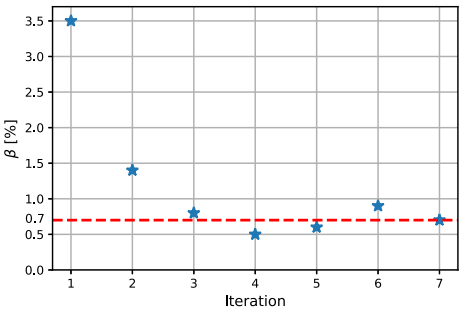

Fig. 4 Relative percentage power variation over different iterations of the Serpent/OpenFOAM coupling. The dashed red line indicates the value of 0.7%, where the coupling converge

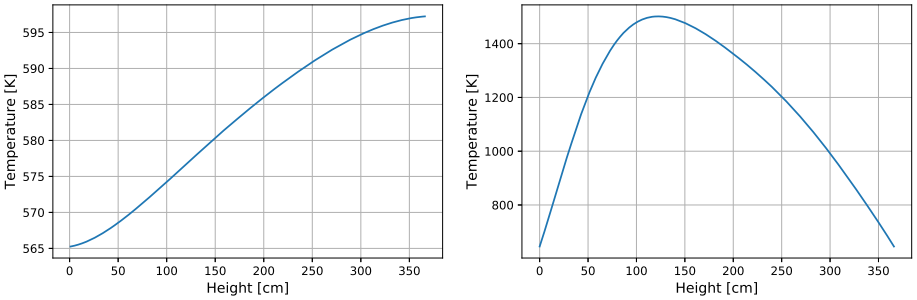

Fig. 5 Temperature profile of average coolant (**a**) and fuel centreline (**b**), from the bottom (0 cm) to the top (366 cm) of the pin, after the convergence of the coupling at fresh fuel in OpenFOAM

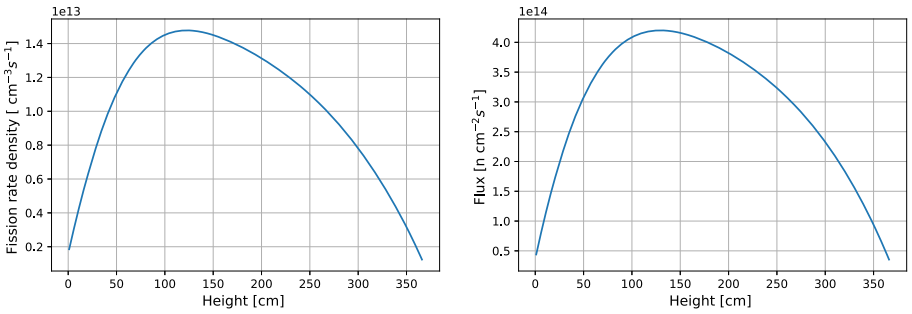

Fig. 6 Fission rate density (**a**) and total neutron flux (**b**) profile, from the bottom (0 cm) to the top (366 cm) of the pin, obtained by the transport calculation in Serpent, after the convergence of the coupling at fresh fuel

4.2 Coupling during the fuel burnup

During the fuel consumption, we update density and temperature fields through the multi-physics coupling at 60, 120, 240 and 365 days. We get a relative power variation under 1% after the convergence, for each time point.

Along the axial direction of the pin, Fig. 7a shows that thermal profile of the water changes slightly during the depletion; differently, in Fig. 7b, the shape of the temperature distribution of the fuel flattens out. The maximum fuel temperature is between 1400 and 1500 K (fresh

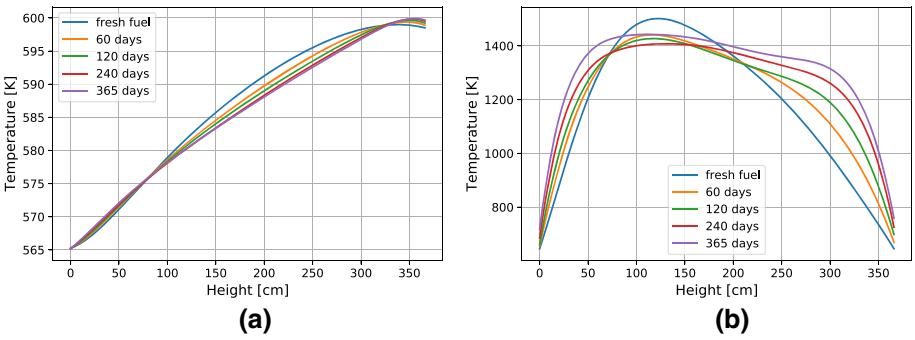

Fig. 7 Temperature profile of average coolant (**a**) and fuel centreline (**b**), from the bottom (0 cm) to the top (366 cm) of the pin, after the convergence of the coupling at fresh fuel, 60, 120, 240 and 365 days in OpenFOAM

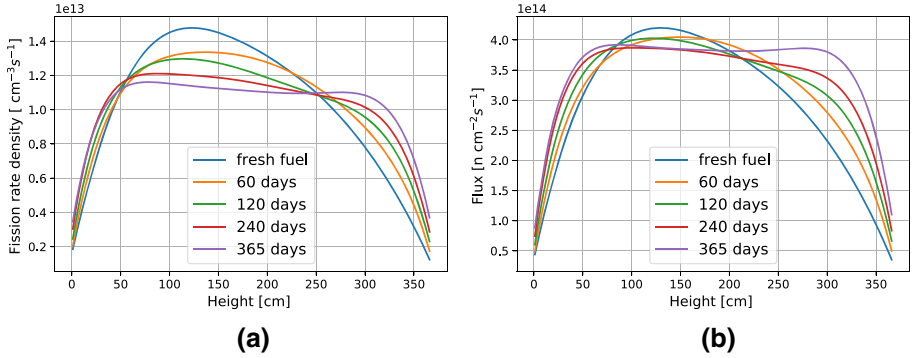

Fig. 8 Fission rate density (**a**) and total neutron flux (**b**) profile, from the bottom (0 cm) to the top (366 cm) of the pin, obtained by the transport calculation in Serpent, after the convergence of the coupling at fresh fuel, 60, 120, 240 and 365 days

fuel), in agreement with the temperatures obtained in [46], referred to the coupling of a PWR mini-assembly geometry with same specific power of the present work.

In the transport calculations, the variation of the thermal hydraulics conditions and burnup affects the neutronics at different time step. In Fig. 8a, the asymmetry of the axial profiles of the fission rate decreases over the time because they flatten out until the end of the burnup history. In Fig. 8b, also the shape of the neutron flux has the same behaviour, but increases over the time. The latter effect is mostly due to the decrease in the multiplication factor k_{eff}, from 1.31160 at fresh fuel to 1.12147 at the end of burnup (uncertainty around 20 pcm), but also to the accumulation of fission products that acts as neutron poisons in the fuel. Indeed, in order to keep constant the power at 65 kW, the total fission rate density remains roughly at the value of $\sim 1.1 \times 10^{13} \text{cm}^{-3}\ \text{s}^{-1}$. The flattening of fission rate and neutron flux is a typical behaviour due to the variation on the composition of the fuel material over the time, as shown in other works [47,48]

4.3 Burnup of the uniform case

We report the results from neutron transport in the uniform case, in order to be compared to the coupled case. Figure 9a shows the distribution of the fission rate at fresh fuel, 60, 120,

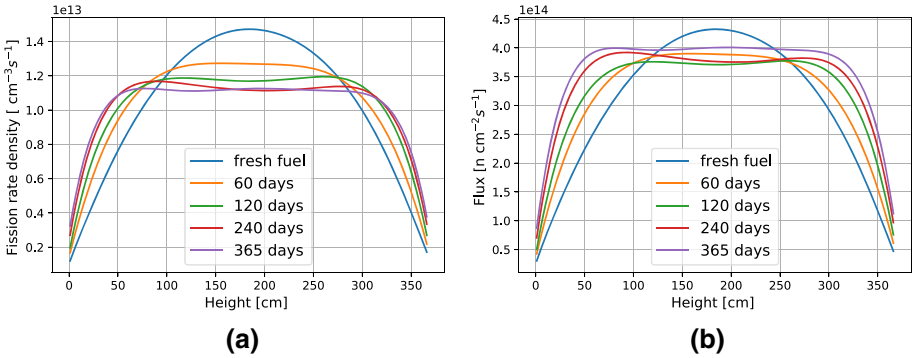

Fig. 9 Fission rate density (**a**) and total neutron flux (**b**) profile along the axial direction of the uniform case

240 and 365 days, along the axial direction. The profile is symmetric for each time step, as expected from the uniform distribution of temperature and density. In Fig. 9b, the neutron flux of the uniform case has the same shape of the fission rate distribution, but increases over the time like in the coupled case. Moreover, we observe also in this case the flattening of the distributions.

The comparison between the uniform and the coupled cases shows differences in axial profiles that may have a non-negligible impact on local fuel burnup, as we show in the next section.

4.4 Fuel burnup along the axial direction

In this section, we show the results of the fuel depletion along the axial direction after 365 days, corresponding to 13.46 MWd/kgU. We calculate the densities for each axial zone from the mean obtained over five radial zones of equal area. The results are obtained from the statistical evaluation over eight independent burnup simulations, in which we get the average values over the concentrations. The relative statistical uncertainties are less than 0.40%.

In order to quantify the effect of the thermal hydraulics feedback on local burnup, we calculate the percentage difference $\Delta n\%$ in nuclide density between coupled and uniform cases in the following way:

$$\Delta n\% = \frac{n_{\text{coupled}} - n_{\text{uniform}}}{n_{\text{uniform}}} \cdot 100 \tag{2}$$

where n_{coupled} and n_{uniform} are the nuclide densities of the coupled and uniform cases, respectively.

4.4.1 Stability of burnup solution

In Sects. 4.2 and 4.3, the shape of the neutron fluxes for both cases suggests the absence of numerical instabilities of the transport calculations. Here we check the stability of the burnup solution from the distribution of ^{135}Xe. Figure 10 shows the axial density distribution of ^{135}Xe for uniform and coupled cases, at 60, 120, 240 and 365 days. On the one hand, the distribution is symmetric for the uniform case at each burnup step. On the other hand, the distribution is slightly asymmetric in coupled case, with a more pronounced asymmetry at 60 days. This effect can be explained by the thermal hydraulics feedback on flux shape. The absence of xenon spatial oscillation (Fig. 3a) confirms the stability of the burnup solution.

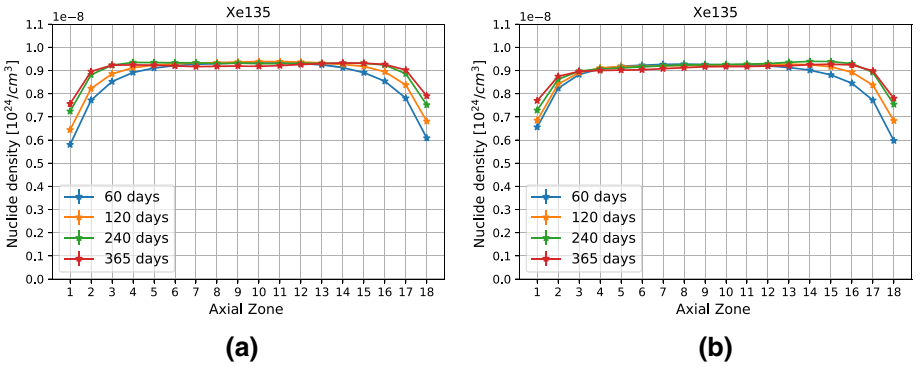

Fig. 10 Nuclide density of ^{135}Xe for uniform (**a**) and coupled (**b**) case along the axial direction at 60, 120, 240 and 365 days. In the x-axis, the index is referred to the ith burnup zone between the bottom and the top of the fuel pin

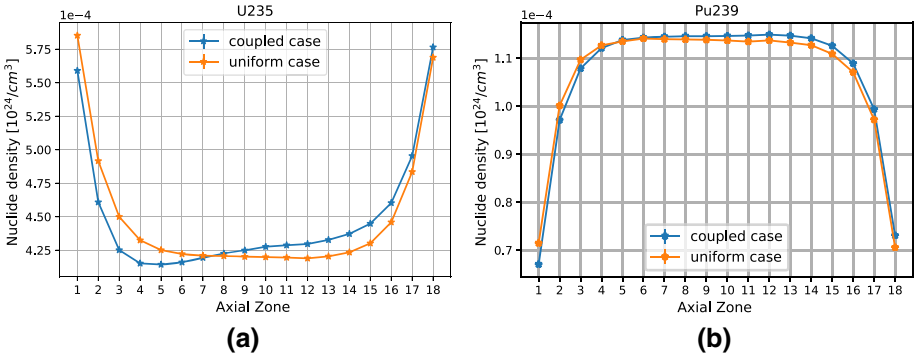

Fig. 11 Nuclide density of ^{235}U (**a**) and ^{239}Pu (**b**) along the axial direction after 365 days of burnup, for coupled (blue line) and uniform (red line) case. In the x-axis, the index is referred to the ith burnup zone between the bottom and the top of the fuel pin

4.4.2 Fuel burnup of ^{235}U and ^{239}Pu

Figure 11a and b shows the nuclide density of ^{235}U and ^{239}Pu for each axial zone of the two cases, after 365 days. In the coupled case, the fissile nuclides have higher consumption in the lower half of the pin. This part corresponds to the region where the moderation is greater, giving the evidence that the axial consumption depends on the neutron thermalization of the coolant. In the uniform case, as expected, the depletion is symmetric along the axial direction.

The differences between the two cases are listed in Table 3. Local differences are greater than 5% for some axial zones of both nuclides. The maximum difference, equal to 6.56%, is found in the lower zone (1st) for ^{239}Pu.

4.5 Fuel burnup along the radial direction

Along the radial direction, we obtain the density field for each radial zone calculating the mean over 18 axial zone of equal length. From the eight burnup independent simulations, the statistical uncertainties on nuclide concentrations are less than 0.0005% for ^{238}U and less than 0.04% for ^{239}Pu.

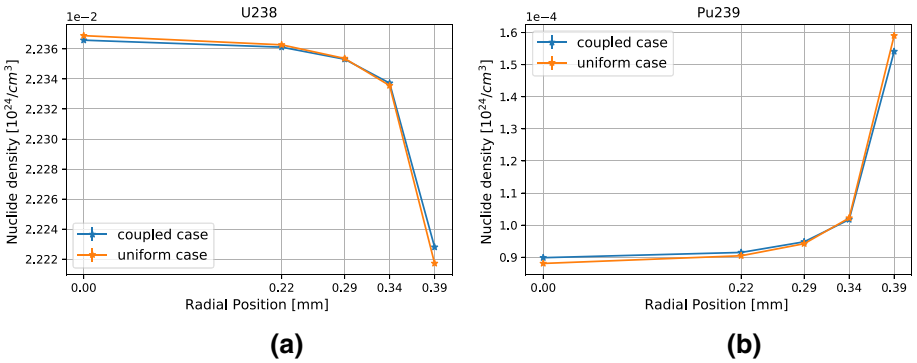

Fig. 12 Nuclide density of ^{238}U (**a**) and ^{239}Pu (**b**) along the radial direction after 365 days for coupled (blue line) and uniform (red line) case. The x-axis reports the distances between the centre of the fuel pin and the centre of each radial region

Figure 12a and b shows the nuclide density of ^{238}U and ^{239}Pu for each radial zone in the two cases, after 365 days of burnup. The dominant effect on fuel depletion is the self-shielding. The neutrons with energies at the resonances of ^{238}U capture cross section are mostly absorbed by the outer fuel layers. As a consequence, ^{238}U is more consumed and ^{239}Pu accumulates more in the outer layer. This effect occurs for both coupled and uniform cases because it is a geometrical effect.

However, some differences show up by comparing the coupled versus the uniform case. In the coupled case, higher fuel temperature in the centre of the pin increases the resonance absorption of neutrons by ^{238}U, due to the Doppler broadening (Fig. 12a). This causes higher production of ^{239}Pu in the centre of the pin (Fig. 12b).

The numerical differences between the coupled and uniform cases are listed in Table 4. The variation of nuclide densities between the two cases is less than 0.04% for ^{238}U and up to 3.09% for ^{239}Pu. The small differences for ^{238}U are due to the fact that this nuclide is present with high concentration in fresh fuel, so the relative consumption is lower with respect to the initial amount of nuclide. On the other hand, ^{239}Pu is generated during the fuel consumption, justifying higher differences.

The effect of the coupling on fuel consumption along the radial direction, as seen along the axial direction, is not negligible. Therefore, the results arise the importance of thermal hydraulics feedback for local fuel consumption.

4.6 Fuel burnup for global concentrations

In order to evaluate the global effect on fuel depletion, we calculate the average nuclide concentrations in all 90 burnup zones. Figure 13a and b shows the global density over time for uniform and coupled cases, until the end of burnup. The relative statistical uncertainties of density for both cases are less than 0.1%. At the end of the burnup history, $\Delta n\%$ is 0.4% for ^{235}U and 0.1% for ^{239}Pu.

We point out that these differences are obtained in a simplified fuel cell. In the future, it would be interesting to evaluate the global effects on fuel assembly and full-core design. Indeed, a different scenario may emerge since, depending on the position, the pins are subject to different thermal hydraulics conditions.

Table 3 $\Delta n\%$ of ^{235}U and ^{239}Pu for each axial zone, after 365 days

	1	2	3	4	5	6	7	8	9	10	11	12	13	14	15	16	17	18
U-235	− 4.48	− 6.26	− 5.51	− 4.00	− 2.54	− 1.46	− 0.37	0.43	1.12	1.84	2.19	2.56	2.93	3.25	3.41	3.22	2.46	1.35
Pu-239	− 6.56	− 3.09	− 1.68	− 0.51	0.26	0.17	0.44	0.59	0.65	0.82	1.10	1.05	1.26	1.5	− 3.22	1.69	2.18	3.41

Table 4 $\Delta n\%$ of ^{238}U and ^{239}Pu for each radial zone, after 365 days

Nuclide	Zone 1	Zone 2	Zone 3	Zone 4	Zone 5
U-238	−0.01	−0.01	−0.00	0.01	0.01
Pu-239	2.04	1.14	0.63	−0.47	−3.09

Fig. 13 Global nuclide density of ^{235}U and ^{239}Pu over a year of burnup for coupled (blue line) and uniform (red line) case

Table 5 Typical computational time for burnup in Serpent and coupling in one iteration for Serpent and OpenFOAM

Simulation	Time (min)
Burnup uniform case Serpent	30
Burnup coupled case Serpent	60
Coupling iteration Serpent (criticality)	25
Coupling iteration OpenFOAM	15

4.7 Computational cost and future extension of this work

We run the simulations on a Linux-based cluster with 2.3 GHz Xeon E5 series processors and 128 GB of RAM. The execution in Serpent is carried out by a hybrid parallel mode on nine nodes in MPI with 36 cores in OMP, with a total of 144 cores used for each simulation. In OpenFOAM, which is suitable for MPI parallelization and has lower computational cost, we ran simulations with 36 cores.

Table 5 shows that burnup simulations for uniform case have half the computational cost of coupled case. The reason is the increase in the time calculation in Monte Carlo for coupled case, in which the pre-processed cross sections are recalculated by Serpent at different temperatures through the on-the-fly [49] treatment in each mesh cell.

We expect that if we implement the coupling for fuel assembly and full-core study with high fidelity, the computational burden will become impracticable. On the one hand, for burnup calculations, we have to take into account the increase up to millions of burnable regions that affects time and memory requirements. On the other hand, there is also the same problem in CFD calculations, because of the increase in the number of mesh cells up to tens of millions or more. For these reasons, we should adopt reduced order modelling strategies [50], as in [51], and simplification of the geometry, as carried out in [26]. Indeed,

considering the symmetry of the geometry and proper boundary conditions, it is possible to simulate sub-assembly and part of the core instead of full geometries. Moreover, we have to carry out grid independence study to use the minimum number of mesh cells and burnup regions for a determined geometry, in order to preserve the accuracy of results.

Finally, pin-by-pin simulations of assemblies and parts of the core can be replaced by a porous medium approach [52] that will reduce computational burden. Future efforts will be devoted to the application of the porous medium approach for burnup analysis of assemblies and full cores.

5 Conclusion

In this paper, we presented a multi-physics modelling approach for 3D burnup analysis, based on the coupling between Serpent for neutronics and OpenFOAM for thermal hydraulics.

We tested the approach adopting a PWR fuel cell as test case. For demonstration purposes, we ran two burnup calculations that cover 365 days for the aforementioned case study. In one calculation, the coupled one, we imported temperature and density fields from OpenFOAM; in the other, the uniform one, we set uniform values. In both calculations, the fuel pin is divided into 5 radial zones of equal area and 18 axial zones of equal length. The results show that the axial profile of the neutron fluxes changes between the two cases for different burnup steps. This effect is due to a different distribution of the fission rate, depending on the temperature distribution of the coolant that moderates more the neutrons in the lower part of the pin. In this way, along the axial direction, the depletion of ^{235}U and ^{239}Pu is asymmetric for the coupled case, with local differences higher than 5% with respect to the uniform case. Along the radial direction, the fuel burnup is influenced by the temperature distribution of the fuel. In the coupled case, neutron captures by ^{238}U are increased in the centre of the pin due to Doppler broadening at high temperatures. This influences the production of ^{239}Pu with local differences in a few percentages between the two cases. Finally, for global densities, the differences are less than 0.5% for ^{235}U and ^{239}Pu at the end of the burnup history.

The results show that the effects of the multi-physics coupling are significant for local burnup, highlighting the importance to develop multi-physics models for burnup analysis. However, even though variations are negligible for global burnup, it should be noted that the case study is a PWR fuel cell, where we do not consider other effects such as control rods, position inside the reactor core and change in thermal power. For this reason, it would be interesting to evaluate global and local effects on burnup for pins in fuel assembly and full-core geometries.

It follows that in future developments of this activity, we plan to implement the methodology for assembly design, allowed thanks to the high flexibility of Monte Carlo for neutronics and CFD for thermal hydraulics. In this case, a critical aspect is the increase in computational cost. To overcome the issue, like in [51] and [26], we can adopt reduced order modelling strategies and consider symmetry of the geometry and proper boundary conditions to simulate sub-assembly and part of the core, instead of full geometries. Furthermore, grid independence studies can be carried out to use the minimum number of mesh cells and burnup regions for a determined geometry.

Finally, we plan to investigate the adoption of a porous medium approach, which will decrease the computational cost without affecting the accuracy of results.

Acknowledgements This work has been supported by CINECA Supercomputing Center, using the GALILEO cluster in Bologna (Italy), and by an Amazon Web Services (AWS) in Education grant award.

References

1. A.G. Mylonakis, M. Varvayanni, N. Catsaros, P. Savva, D.G.E. Grigoriadis, Ann. Nucl. Energy **72**, 104 (2014)
2. A. Cammi, V. Di Marcello, L. Luzzi, V. Memoli, *A Multi-Physics Modelling Approach Oriented to Safety Analysis of Innovative Nuclear Reactors* (Nova Science Publishers, Hauppauge, 2011)
3. A. Cammi et al., Ann. Nucl. Energy **38**, 1356 (2011)
4. E. Cervi, S. Lorenzi, A. Cammi, L. Luzzi, Nucl. Eng. Des. **346**, 209 (2019)
5. E. Cervi, S. Lorenzi, L. Luzzi, A. Cammi, Ann. Nucl. Energy **132**, 227 (2019)
6. J. Leppänen, M. Pusa, T. Viitanen, V. Valtavirta, T. Kaltiaisenaho, Ann. Nucl. Energy **82**, 142 (2015)
7. J.F. Briesmeister, MCNP—A General Monte Carlo N-Particle Code, Version 4C (LA-13709-M., Los Alamos National Laboratory, 2000)
8. E. Shwageraus, E. Fridman, E. Abramski, A. Galperin, in *The 23th Conference of the Nuclear Societies in Israel Book of articles* (Israel, 2006), p. 256
9. D.P. Griesheimer, Ann. Nucl. Energy **82**, 29 (2015)
10. K. Wang et al., Ann. Nucl. Energy **82**, 121 (2015)
11. V. Valtavirta, T. Viitanen, J. Leppänen, Nucl. Sci. Eng. **177**, 193 (2014)
12. D. Kotlyar, Y. Shaposhnik, E. Fridman, E. Shwageraus, Nucl. Eng. Des. **241**, 3777 (2011)
13. D.P. Griesheimer et al., Ann. Nucl. Energy **82**, 29 (2015)
14. J. Leppanen, T. Viitanen, V. Valtavirta, Trans. Am. Nucl. Soc. **1074**, 1165–1168 (2012)
15. Lin-Sen Li, Hao-Min Yuan, Kan Wang, Nucl. Eng. Des. **250**, 385 (2012)
16. A. Ivanov, V. Sanchez, U. Imke, Development of a Coupling Scheme Between MCNP5 and SUBCHANFLOW for the Pin- and Fuel Assembly-Wise Simulation of LWR and Innovative ReactorsM&C 2011 (Rio de Janeiro, Brazil, May 8–12, 2011)
17. D. Kotlyar, E. Shwageraus, Ann. Nucl. Energy **63**, 371 (2014)
18. J. Dufek, J.E. Hoogenboom, Nucl. Sci. Eng. **162**, 307 (2009)
19. L. Jutier et al., Nucl. Sci. Eng. **181**, 105 (2015)
20. A. Cammi et al., Nucl. Eng. Des. **300**, 308 (2016)
21. D. Chiesa, M. Clemenza, S. Pozzi, E. Previtali, M. Sisti et al., Ann. Nucl. Energy **96**, 270 (2016)
22. H.G. Weller, G. Tabor, H. Jasak, C. Fureby, Comput. Phys. **12**, 620 (1998)
23. https://openfoam.org/
24. C. Castagna et al., in *Proceedings of 26th International Conference Nuclear Energy for New Europe* (Bled, Slovenia, September 11–14, 2017), pp. 603.1–603.8
25. C. Castagna et al., in *Proceedings of Physor 2018* (Cancún, México, April 22–26, 2018) pp. 2115–2125
26. C. Castagna, S. Lorenzi, A. Cammi, in *Proceedings of 27th International Conference Nuclear Energy for New Europe* (Portoroz, Slovenia, September 10–13, 2018), pp. 205.1–205.8
27. G. Grasso, C. Petrovich, D. Mattioli, C. Artioli, P. Sciora, D. Gugiu, G. Bandini, E. Bubelis, K. Mikityuk, Nucl. Eng. Des. **278**, 287 (2014)
28. A. Bousbia-Salah, F. D'Auria, Prog. Nucl. Energy **49**, 1 (2007)
29. C. Castagna, D. Chiesa, A. Cammi, S. Boarin, E. Previtali, M. Sisti, M. Nastasi, A. Salvini, G. Magrotti, M. Prata, Ann. Nucl. Energy **113**, 171 (2018)
30. R. Eymard, T. Gallouet, R. Herbin, *The Finite Volume Method. Handbook for Numerical Analysis* (North Holland, Amsterdam, 2000), pp. 715–1022
31. O.C. Zienkiewicz, R.L. Taylor, P. Nithiarasu, *The Finite Element Method for Fluid Dynamics* (Elsevier, Butterworth-Heinemann, Amsterdam, 2013)
32. The Westinghouse Pressurized Water Reactor nuclear power plant (Westinghouse Electric Corporation Water Reactor Divisions, 1984)
33. T.L. Perelman, Int. J. Heat Mass Transf. **3**, 293 (1961)
34. Internal Assessment for the Properties of Water and Steam. Revised Release on the IAPWS Industrial Formulation 1997 for the Thermodynamic Properties of Water and Steam. Technical Report (International Association for the Properties of Water and Steam, 2007)
35. J.R. Lamarsh, *Introduction to Nuclear Engineering* (Addison-Wesley, Boston, 1975)
36. W.G. Luscher, K.J. Geelhood, Material Property Correlations: Comparisons Between FRAPCON-3.4, FRAPTRAN 1.4, and MATPRO. Technical Report. NUREG-CR-7024 (Pacific Northwest National Laboratory, 2011)
37. S.B. Pope, *Turbulent Flows* (Cambridge University Press, Cambridge, 2000)
38. D.B. Spalding, J. Appl. Mech. **28**, 455 (1961)
39. W. B. Weihermilfer, C. S. Allison, LWR Nuclear Fuel Bundle Data for Use in Fuel Bundle Handling. Topical Report EY-76-C-M-1830 (Pacific Northwest Laboratory, 1979)
40. A.E. Isotalo, P.A. Aarnio, Ann. Nucl. Energy **37**, 1987 (2011)

41. OECD/NEA Data Bank, The JEFF-3.1.1 Nuclear Data Library. Technical Report 22, 2009
42. J.R. Lamarsh, *Introduction to Nuclear Reactor Theory* (Addison-Wesley Publishing Company, Boston, 1966)
43. J. Dufek, D. Kotlyar, E. Shwageraus, Ann. Nucl. Energy **60**, 295 (2013)
44. J. Dufek, D. Kotlyar, E. Shwageraus, Ann. Nucl. Energy **62**, 260 (2013)
45. H. Robbins, S. Monro, Ann. Math. Stat. **22**, 400 (1951)
46. D. Kotlyar, E. Shwageraus, Ann. Nucl. Energy **96**, 61 (2016)
47. F. Gleicher et al., in *Proceedings of Top Fuel 2016* (Boise, ID, USA, September 11–15, 2016), pp. 261–270
48. H.S. Jeong et al., Ann. Nucl. Energy **90**, 240 (2016)
49. T. Viitanen, J. Leppänen, Nucl. Sci. Eng. **171**, 165 (2012)
50. G. Rozza, D.B.P. Huynh, A.T. Patera, Arch. Comput. Methods Eng. **15**, 229 (2008)
51. C. Castagna, M. Aufiero, S. Lorenzi, G. Lomonaco, A. Cammi, Energies **13**(4), 1 (2020)
52. C. Fiorina, I. Clifford, M. Aufiero, K. Mikityuk, Nucl. Eng. Des. **294**, 24 (2015)